Chinese Chemical Letters 34 (2023) 108056

Contents lists available at ScienceDirect

Chinese Chemical Letters

journal homepage: www.elsevier.com/locate/cclet

# N-doped graphitic carbon encapsulating cobalt nanoparticles derived from novel metal–organic frameworks for electrocatalytic oxygen evolution reaction

Yuanmeng Tian[a,b,c], Hao Wu[d], Aamir Hanif[b], Yanli Niu[a], Ying Yin[a], Yangyi Gu[a], Zuofeng Chen[a], Qinfen Gu[e], Yun Hau Ng[b,c,*], Jin Shang[b,c,*], Liangchun Li[a,*], Mingxian Liu[a]

[a] Shanghai Key Lab of Chemical Assessment and Sustainability, School of Chemical Science and Engineering, Tongji University, Shanghai 200092, China
[b] School of Energy and Environment, City University of Hong Kong, Hong Kong SAR 999077, China
[c] City University of Hong Kong Shenzhen Research Institute, Shenzhen 518000, China
[d] Macao Institute of Materials Science and Engineering, Faculty of Innovation Engineering, Macau University of Science and Technology, Macau SAR 999078, China
[e] Australian Synchrotron (ANSTO), Victoria 3168, Australia

ARTICLE INFO

*Article history:*
Received 31 October 2022
Revised 29 November 2022
Accepted 9 December 2022
Available online 11 December 2022

*Keywords:*
Metal-organic frameworks
Oxygen evolution reaction
High nitrogen content
Cobalt nanoparticles
Hierarchical structure

ABSTRACT

Nitrogen-doped carbon catalysts with hierarchical porous structure are promising oxygen evolution reaction (OER) catalysts due to the faster mass transfer and better charge carrying ability. Herein, an exquisite high nitrogen-containing ligand was designed and readily synthesized from the low-cost biomolecule adenine. Accordingly, three new MOFs (TJU-103, TJU-104 and TJU-105) were prepared using the Co(II) or Mn(II) ions as metal nodes. Through rationally controlling pyrolysis condition, in virtue of the high nitrogen content in well-defined periodic structure of the pristine MOFs, TJU-104–900 among the derived MOFs with hierarchical porous structure, *i.e.*, N-doped graphitic carbon encapsulating homogeneously distributed cobalt nanoparticles, could be conveniently obtained. Thanks to the synergistic effect of the hierarchical structure and well dispersed active components (*i.e.*, C=O, Co–$N_x$, graphitic C and N, pyridinic N), it could exhibit an overpotential of 280 mV@10 mA/cm$^2$ on carbon cloth for OER activity. This work provides the inspiration for fabrication of nitrogen-doped carbon/metal electrocatalysts from cost-effective and abundant biomolecules, which is promising for practical OER application.



The rapid depletion of traditional fossil fuels and the emission of greenhouse gasses from their combustion have stimulated the development of clean energy conversion systems. Advanced systems for clean energy generation and storage such as water splitting [1–4], fuel cells [5] and metal-air batteries [6,7] are promising in addressing the energy and environmental challenges. These technologies involve several key electrochemical reactions, which could convert the chemical energy into electrical energy or store the energy. Oxygen evolution reaction (OER), as one of the critical reactions at the anode of an electrolytic cell, is the oxidation of water or hydroxyl ions on the surface of catalysts to generate gaseous oxygen [8]. The sluggish reaction kinetics restricts its energy efficiency, which requires a substantial overpotential to drive the OER [9]. Noble metal oxides (*e.g.*, $IrO_2$/$RuO_2$) are considered as the most efficient OER catalysts [10]. However, their scarcity, high cost, and instability limit their practical applications [1]. In this regard, it is highly imperative to develop more cost-effective and environment-friendly alternative OER catalysts containing base metals (cobalt, nickel, iron, *etc.*) [11–14].

Metal–organic frameworks (MOFs) or porous coordination polymers (PCPs) with base metals and their derivatives are desirable candidates for electrocatalysis from the economic and performance views [15–20]. Their structural designability and composition adjustability allow for achieving high OER performance [1,20–22]. Rational design of the structures and compositions of MOFs or their derivatives could attain more active sites, faster ion transportation, and lower internal resistance to elevate the OER activity [20,21,23]. Recently, doping heteroatoms (nitrogen, boron, sulfur, and phosphorus) into MOFs for enhancing the OER activity has been garnering increasing attention [20,24]. The high electronegativity of heteroatoms could influence the electronic structure to enhance the intrinsic activity of active sites [25–28]. In particular, electron-

* Corresponding authors.
*E-mail addresses:* yunhau.ng@cityu.edu.hk (Y.H. Ng), jinshang@cityu.edu.hk (J. Shang), lilc@tongji.edu.cn (L. Li).

https://doi.org/10.1016/j.cclet.2022.108056
1001-8417/

withdrawing nitrogen atoms (*e.g.*, pyridinic N) may cause positively charged carbon in a $\pi$–system to facilitate the charge transport process thus favoring OER activity [29].

Most researches have focused on developing the N-containing carbon electrocatalysts with homogeneously atoms dispersion derived from pristine MOFs with endogenous N content (*e.g.*, ZIFs series have N-containing organic linkers) or exogenous heteroatom sources (*e.g.*, pyrolysis under $NH_3$ atmosphere) [30–34]. Deriving the N-doped carbon material from pristine MOFs with N content *via* proper one-step pyrolysis is a more expedient way, benefited from the well-defined porous structure, which could afford hierarchical composites to drive a good OER activity. The coordination between metal and nitrogen could prevent aggregation of the materials to some extent during pyrolysis process [23]. On the other hand, the derived materials could inherit the accessibility of active sites from the original porous structure of pristine MOFs and obtain additional N-doped carbonaceous matrix as active components from organic ligands. However, the novel N-containing pristine MOFs are rare, some of them (*e.g.*, ZIF-67) have been widely used for OER activity. Still very few of them could provide active sites to drive OER reactions efficiently suffering from low conductivity, which also restricts the MOFs with prominent OER performances [35]. Thus, new ligands for novel MOFs are urgently needed to diversify the MOFs structures, and the newly developed MOFs can serve as good self-sacrificial precursors to fabricate hierarchical derivatives and broaden their availability for electrochemical activity. It is highly desirable to design a rigid and regularly arranged $\pi$-conjugated ligand with high N content in combination with base metals to assemble novel MOFs, which could potentially produce homogeneous precise N-doping material with conceived morphologies and compositions favoring the OER activity [36].

Herein, we synthesized three new MOFs (denoted as TJU-103, TJU-104 and TJU-105) using a high nitrogen-content ligand (TAP) synthesized from a cheap and green biomolecule adenine and converted the MOFs to the derived carbon materials for systematical investigation on their OER activity. Pristine MOF TJU-104 exhibited the best OER performance among three pristine MOFs, which possesses more accessible cobalt as metal active sites (MASs) than that of nonporous TJU-103 and outperforms its isostructural TJU-105 with manganese as MASs. Subsequently, a novel MOF-derived catalyst (TJU-104–900) inheriting the porous structure of TJU-104 with the accessibility of active sites could be easily obtained *via* one-step pyrolysis from the well-defined structure. The TJU-104–900 possesses a hierarchical structure (nano-metal particles encapsulated by N-doped graphitic carbons) featuring single cobalt atoms, active Co–$N_x$ components, and functional groups, which can drive a good OER activity with an overpotential of 280 mV@10 mA/cm$^2$ on the carbon cloth. The systematic investigations disclose that the high N content linkers could improve the inherent conductivity and facilitate the production of homogeneously N-doped carbon material to generate active components for efficient OER catalysts.

A new ligand TAP (6-(4*H*-1,2,4-triazol-4-yl)–7*H*-purine, supporting information) possessing seven nitrogen atoms (*i.e.*, N content as high as 52.4 wt%) was synthesized *via* one-step facile modification of the low-cost biomolecule Adenine, as verified by NMR (Scheme S1, Figs. S1 and S2 in Supporting information). Subsequently, three new MOFs (TJU-103, TJU-104, TJU-105) were successfully prepared by solvothermal reactions of TAP with $Co(NO_3)_2$ or $Mn(NO_3)_2$. The structures of the three pristine MOFs were obtained from Single-crystal X–ray diffraction (Fig. 1, Table S1 and Figs. S3–S5 in Supporting information). TJU-103 has a nonporous structure that crystallizes in R–3c space group with $Co^{2+}$ as metal nodes bonded by six N atoms of the ligands (Figs. 1a and d, Fig. S3 and Table S1). TJU-104 has a completely different structure featuring an ionic skeleton (balanced by $OH^-$ anions) in a 3D porous structure that crystallizes in P 63 space group with each $Co^{2+}$ coordinated by one $\mu_3$–OH, one $H_2O$ molecule, and four N atoms of the ligands (Figs. 1b and e, Fig. S4 and Table S1). TJU-105 is isostructural of TJU-104 except that the metal ions are $Mn^{2+}$ instead of $Co^{2+}$ (Figs. 1c and f, Fig. S5 and Table S1).

Given MOF derived material could simultaneously possess better stability and more promising active components for OER activity, N-doping-carbon/metal hierarchical nanostructure materials were successfully fabricated from the as-prepared pristine MOFs *via* pyrolysis. Considering Co is one of the promising transition metals (*i.e.*, Fe, Co, Ni) benefiting to electrochemical activity [20], and the existence of $OH^-$ in TJU-104 framework has potential as the reaction-intermediate for OER activity, we first pyrolyzed it at three different temperatures (800, 900, 1000 °C) as graphitic structures usually are prepared by thermal pyrolysis at high temperatures (≥ 800 °C), and the carboreduction process generally proceeds intensely at a higher temperature (∼1000 °C) for producing single cobalt atom to facilitate OER activity [37,38]. The pyrolysis temperature of 900 °C has been proved to be proper for the synthesized MOFs due to the existence of graphitized carbon as evidenced by powder X–ray diffraction (PXRD). The hierarchi-

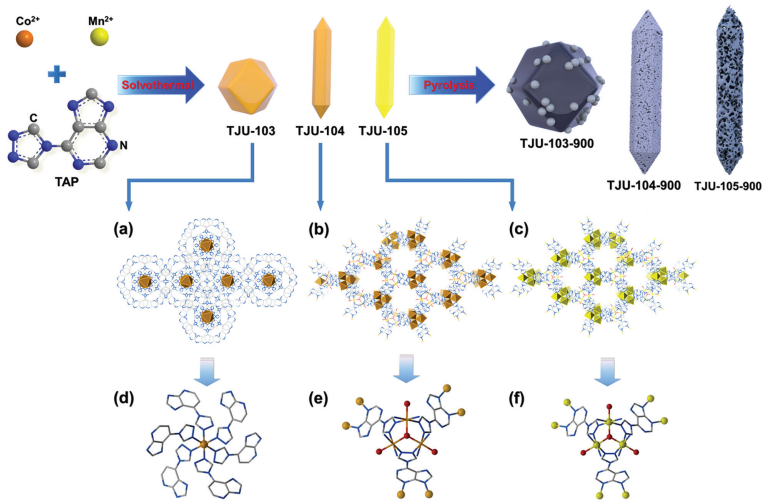


**Fig. 1.** Schematic illustration of the preparation of electrocatalysts with high N content and single-crystal structure of (a, d) TJU-103, (b, e) TJU-104 and (c, f) TJU-105 (gray: C atom, red: O atom, blue: N atom, orange: Co atom, yellow: Mn atom).

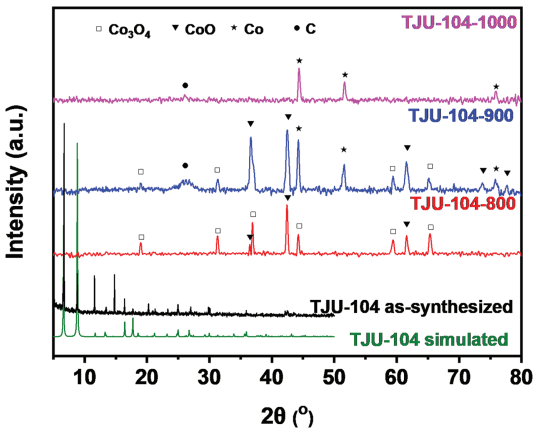


**Fig. 2.** XRD patterns of TJU-104 and TJU-104–800/900/1000 ($Co_3O_4$: JCPDS No. 74–2120, CoO: JCPDS No. 71–1178, Co: JCPDS No. 15–1806).

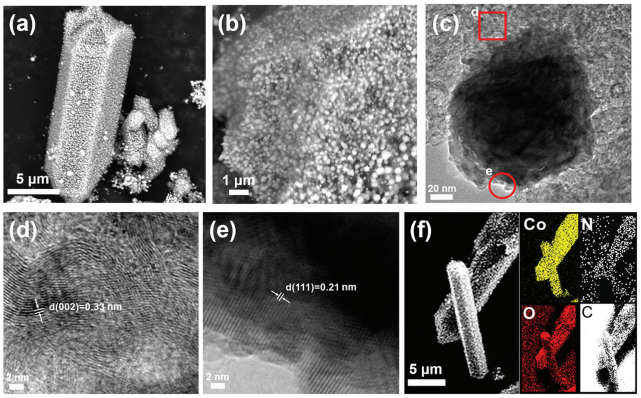


**Fig. 3.** (a, b) SEM images, (c) TEM image, (d, e) HR–TEM images, (f) EDX elemental mapping images of TJU-104–900.

cal porous structure can be further verified by scanning electron microscopy (SEM) and transmission electron microscopy (TEM). As shown in Fig. 2, in TJU-400–900 the peak at $2\theta \approx 26°$ reveals that the graphitized carbon is prone to form at 900 °C [33]. The phases of TJU-104–900 are metallic Co ($2\theta \approx 44.4°$, 52.7°, 76.0°, JCPDS No. 15–0806), CoO, and a little $Co_3O_4$ [39,40]. Herein, $Co_3O_4$ and CoO are partially changed from 800 °C, and they will further transfer to metallic Co phases at 1000 °C due to the reduction by decomposition of the N-heteroatom organic ligands under higher temperature [33]. Notably, TJU-104–900 manifests a 3D interconnected porous structure with uniform spherical particles size (~200 nm) shown in Figs. 3a and b, which is quite different from TJU-104–800 and TJU-104–1000 with noticeable agglomerations (Figs. S6 and S7 in Supporting information). The selected particle (*ca.* 160 nm) of TJU-104–900 shows the inter-planar spacing of 0.21 nm and 0.33 nm, which were assignable to Co(111) and graphitized carbon (002), respectively (Figs. 3c–e) [33]. Moreover, the C, N, Co and O elements were found to be evenly distributed on the TJU-104–900 surface according to the elemental mapping images (Fig. 3f). Combining the TEM profile shown in Fig. 3c, TJU-104–900 manifests a unique structure that uniform nano-cobalt particles are encapsulated in N-doped graphitic carbons, which could endow interactions between C–N sites and nano-metal particles and good stability, being potentially advantageous for OER [25,41].

To evaluate the porosity of these hierarchical structures, Brunauer–Emmett–Teller (BET) surface area measurements were conducted. It was found that the TJU-104–900 possesses the largest surface area among the TJU-104-derived materials and features abundant micropores and mesopores, verified by the $N_2$ sorption and pore distribution curves (Fig. S8 and Table S3 in Supporting information). This can be attributed to its unique morphology, which is different from the obvious agglomerations of TJU-104–800 and TJU-104–1000 (Figs. S6 and S7 in Supporting information). Based on the above discussion, it indicates that adjusting the pyrolysis temperatures of the same parent structure can trigger distinct thermal reactions to form intriguing structures with completely different compositions [42,43].

To the best of our knowledge, N-doped graphitized carbons and hierarchical porous structures could boost electrocatalysis in virtue of the resulting charge redistribution, new active MASs, *etc.* [44–46]. Combined with literature and the above experimental results of TJU-104, hierarchical porous structure with graphitic carbon can be produced by one-step at the optimal temperature (900 °C). Thus, apart from the TJU-104 derived samples, we prepared TJU-103–900 and TJU-105–900 as potential electrocatalysts for comparison, which were pyrolyzed at 900 °C from TJU-103 and TJU-105, respectively. Analysis of the PXRD patterns of TJU-103–900 and TJU-105–900 (Figs. S9 and S10 in Supporting information) revealed the absence of peaks at $2\theta \approx 26°$, suggesting the absence of the graphitized carbon. TJU-103–900 possesses metallic cobalt instead of cobalt oxides mainly due to the absence of O element in the framework of TJU-103. TJU-105–900 possesses mixed components of MnO and $Mn_3O_4$. As shown in the SEM images (Figs. S12 and S14 in Supporting information), TJU-103–900 displays agglomeration, and TJU-105–900 exhibits cracks and macro-cavities. It suggests that the compositions and structures of the derived MOFs are fully governed by the parent pristine MOFs in the same pyrolysis condition. The reduction of the metal nodes by the organic ligand along with the carbonization of the organic ligands could generate distinct inorganic hierarchical composites during pyrolysis processes.

The novel pristine MOFs were examined first for the electrocatalytic oxygen evolution reactions, which were carried out using a standard three-electrode system with 1.0 mol/L KOH as the electrolyte by glassy carbon (GC) electrode. Commercial $RuO_2$ and ZIF-67 were used as benchmark catalysts for comparison. The TJU MOFs (except for TJU-105) with high nitrogen content in the frameworks exhibited much better electrocatalytic performance than $RuO_2$ according to linear sweep voltammetry (LSV) curves (Fig. 4a). The poor performance of TJU-105 is attributed to the lower activity of Mn as the metal nodes (Figs. S4 and S5), which is consistent with the activity of transition metals in the order of Co > Fe > Mn [47]. Notably, the pristine TJU-103 and TJU-104 crystals in micron size (Figs. S11 and S13 in Supporting information) showed a lower overpotential ($\eta$, 380 and 350 mV) to drive the current density ($j$) of 10 mA/cm$^2$ and smaller Tafel slope (78 and 74 mV/dec), exhibiting an evidently better OER activity compared to the similar MOFs (cobalt as the metal nodes and using pristine MOFs for OER activity) such as nano-sized MAF-X27-OH, $TiC_2$TX-CoBDC, ZIF-67, micron-sized Co-MOF-74 and ZIF-9 (Table S2 in Supporting information) [48]. It could be ascribed to the cobalt nodes and high N content (including the pyridinic N) of the TAP ligands. The easily synthesized ligand (TAP) with a high N content has a lower HOMO–LUMO gap than other N containing ligands (*e.g.*, 2-methylimidazole in ZIF-67 with 34.1 wt% N content; benzimidazole in ZIF-9 with 23.7 wt% N content) verifying by Gaussian (Fig. S15 in Supporting information), which could contribute to a good electrical conductivity and simultaneously serve as a good N source for OER activity.

Of the pristine MOFs examined in this study, TJU-104 exhibited the best OER performance. Its overpotential of 350 mV at 10 mA/cm$^2$ is lower than TJU-103 (380 mV), ZIF-67 (400 mV), and $RuO_2$ (470 mV) (Fig. 2a), and it possessed more efficient active sites for OER activity suggested by a larger double-layer capacitance ($C_{dl}$) value (5.37 mF/cm$^2$) than that of TJU-103 (4.75 mF/cm$^2$) (Fig.

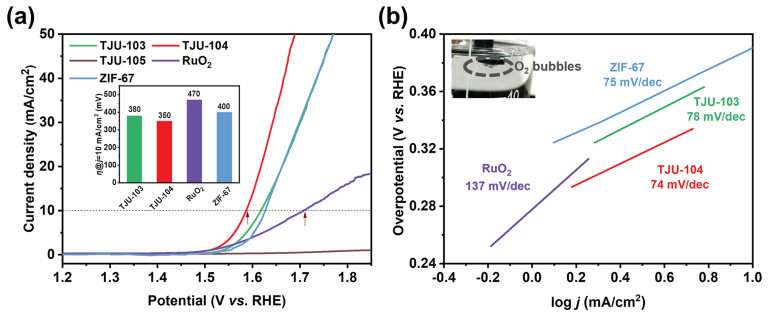


**Fig. 4.** OER performance of the different pristine MOFs and commercial $RuO_2$ (without iR compensation) using GC. (a) LSV curves of the catalysts and commercial $RuO_2$. Inset: overpotential at 10 mA/cm$^2$ density. (b) Tafel plots. The measurement condition of ZIF-67 is in 1 mol/L KOH aqueous solution by using GC as working electrode in the literature [49].

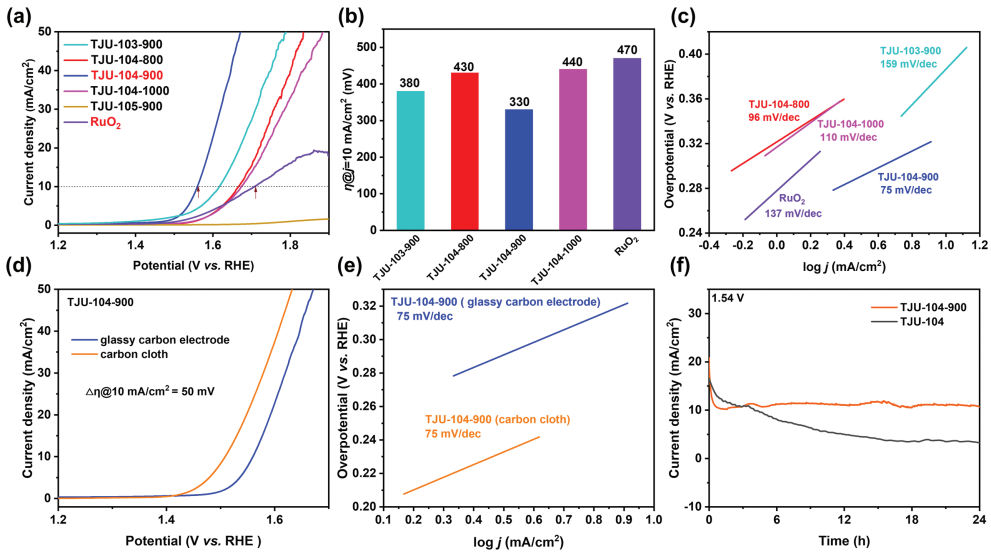


**Fig. 5.** OER performance of the different pristine and derived MOFs and commercial $RuO_2$ (without iR compensation). (a) LSV curves of the catalysts synthesized by different methods or under different pyrolysis temperature. (b) Overpotential at 10 mA/cm$^2$ density. (c) Tafel plots by using GC. (d, e) LSV curves and Tafel plots of TJU-104–900 on GC and CC. (f) The current density *versus* time (*i*–*t*) curves of TJU-104–900 on CC and TJU-104 recorded for 24 h at 1.54 V *vs.* the reversible hydrogen electrode (RHE).

S16 in Supporting information) [50]. Moreover, TJU-104 showed a faster charge-transfer process than TJU-103 as suggested by a much smaller charge transfer resistance ($R_{ct}$, 10 Ω for TJU-104 *vs.* 30 Ω for TJU-103) and faster ion diffusion rate (larger phase angle at low frequency) as shown in the electrochemical impedance spectroscopy (EIS) measurements (Fig. S17 in Supporting information) [51]. The better performance of TJU-104 is attributed to its porous structure and the $OH^-$ groups in its framework. Further insights into the catalytic efficiency of the pristine MOFs were obtained by examining the Tafel slopes. The Tafel slopes of TJU-104 (74 mV/dec) is 4 mV/dec lower than that of TJU-103 (78 mV/dec) and only ca. a half of the $RuO_2$ (137 mV/dec), but close to that of ZIF-67 (75 mV/dec) (Fig. 4b), showing the comparable OER kinetics of ZIF-67, and faster OER kinetics of TJU MOFs than $RuO_2$ which suggest the favorable active sites in TJU MOFs. Even though TJU-103 shows negligible porosity, its performance is not far off that of TJU-104 with porous $CoN_4$ and Co–O coordination structure due to the existence of unique $CoN_6$ coordination mode. Overall, it is supposed that the inherent conductivity of MOFs can be improved by the ultrahigh nitrogen content of linkers, thereby improving the electrocatalytic performance.

The MOFs derived materials were examined for the OER activity by GC (Figs. 5a–c). TJU-104–900 featuring hierarchical composite with the lowest overpotential ($\eta$) of 330 mV stands out among the MOF-derived samples to drive the current density ($j$) of 10 mA/cm$^2$ (Fig. 5b). The $C_{dl}$ value of TJU-104–900 (10.8 mF/cm$^2$) is considerably higher than that of TJU-104–800 (0.77 mF/cm$^2$) and TJU-104–1000 (1.65 mF/cm$^2$) and comparable to that of TJU-103–900 (11.25 mF/cm$^2$), suggesting remarkable electroactive surface area and accessible active sites in TJU-104–900 (Fig. S16). In addition, TJU-104–900 with the smallest EIS semicircle displayed a lower Tafel slope (75 mV/dec) than TJU-104–800 (96 mV/dec), TJU-104–1000 (110 mV/dec), and TJU-103–900 (159 mV/dec), indicating a faster charge transfer and larger OER kinetics (Fig. 5c and Fig. S18 in Supporting information). Notably, TJU-103–900 possessing the highest electroactive surface area manifested the lowest kinetics, *i.e.*, the largest Tafel slope, revealing that these active sites exposed on the surface have low reactivity (Fig. 5 and Fig. S12). This may be mainly ascribed to the agglomeration structure of TJU-103–900.

Given that different working electrode substrates could affect the OER performance, the best-performing TJU-104–900 electrocatalyst was fabricated on conductive carbon cloth (CC, 0.5 cm × 0.5 cm) instead of glassy carbon to explore the potentially further improved OER performance (Figs. 5d–f). To our delight, the $\eta$ was successfully reduced to 280 mV at 10 mA/cm$^2$ with Tafel slope of 75 mV/dec due to the improved electrochemical accessible surface of the carbon cloth [49], and a TOF value of 0.93 s$^{-1}$ was obtained. After 3000$^{th}$ LSV cycle experiments (Fig. S19 in Supporting information), the values of overpotential and Tafel slope have slightly increased. It may be ascribed to the decreased functional groups (C–O at 1040 cm$^{-1}$ in IR spectroscopy, Fig. S20 in Supporting information) and partial agglomeration of the particles

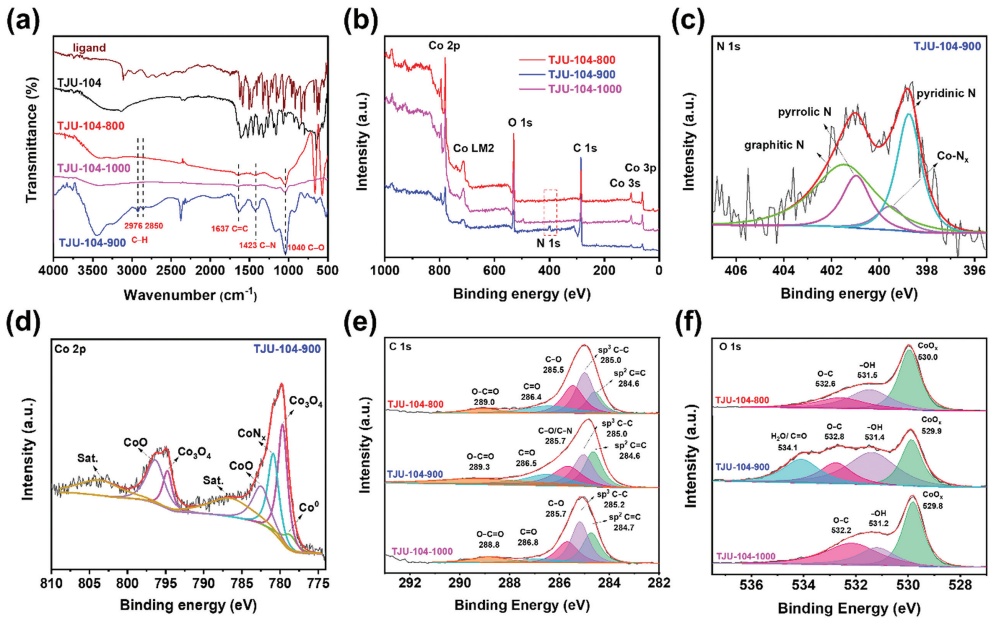


**Fig. 6.** (a) IR spectra, (b) XPS full scan, (c) N 1s XPS spectra, (d) Co 2p XPS spectra, (e) C 1s XPS spectra, and (f) O 1s XPS spectra of TJU-104 and/or its pyrolysis derivatives.

on the surface (Fig. S21 in Supporting information). Nevertheless, during a chronoamperometry measurement at 1.54 V, the current density can retain at around 10 mA/cm$^2$ for 24 h without degradation (Fig. 5f) comparing with an noticeable decrease of the pristine TJU-104 sample due to the dissolution, suggesting the desired improved stability of this MOF-derived OER working electrode.

To understand how TJU-104 derived samples perform superiorly in OER activity, their porous structures and functional groups were identified by $N_2$ gas adsorption at 77 K, IR spectroscopy, and X−ray photoelectron spectroscopy (XPS). TJU-104–900 with well-dispersed cobalt nanoparticles exhibited the largest surface area (143 m$^2$/g, Table S3), which suggests more MASs could be exposed to facilitate the surface reactions. The IR spectra show that C=C at 1637, C–N at 1423, and C–O at 1040 cm$^{-1}$ were detected as functional groups in TJU-104 derived samples (Fig. 6a) [30].

To further reveal the OER activity mechanism, XPS spectra were recorded and the N 1s, C 1s, O 1s, Co 2p binding energies were deconvoluted to gain chemical composition in the bonding and species types. Only TJU-104–900 surface showed exposed N content, and it had significantly higher C, less O and Co content confirmed by the XPS results and the intensity in full XPS spectra (Table S3 and Fig. 6b). Energy-dispersive X−ray (EDX) spectroscopy was further conducted to demonstrate a comparable superficial composition as the XPS of all the TJU-104 derived samples (Table S3). With the pyrolysis temperature increasing the element compositions varied considerably which may be due to the distinct changes of the morphologies and that only the surface compositions were detected by XPS and EDX. The dramatic decline of the nitrogen content could be attributed to its sacrificial function as reducing agent to $Co^{2+}$ metal ions during the pyrolysis. It was consistent with that hierarchical structural TJU-104–900 had a manifestation of N-doped graphitic carbons encapsulating Co nanoparticles. The exposed N content doped in the graphitic carbon matrix influenced the electronic environment of TJU-104–900, favoring the high OER activity. On the other hand, Co–$N_x$ with 7.5% content was discovered in TJU-104–900 that could serve as additional active sites for OER activity (Fig. 6c and Table S4 in Supporting information). Moreover, pyridinic N (398.7 eV) and graphitic N (401.4 eV) dominate the composition with the high content (32.6%, 43.5%, respectively) [52], which could facilitate the interfacial electron transfer and improve the electrical conductivity to obtain superior OER performance [33]. The Co 2p binding energy of TJU-104–900 further confirmed the existence of $CoN_x$ (Fig. 6d and Table S4), and $Co^0$ (778.7 eV, 3.7%), $Co^{3+}$ of $Co_3O_4$ (779.6 eV, 794.8 eV, 27.8%) and $Co^{2+}$ of CoO (782.5 eV, 796.3 eV, 26.0%) which can serve as rich active sites for enhancing OER activity [53]. All TJU-104 derived samples showed the $sp^2$ C=C, $sp^3$ C–C, C–O/C–N, C=O and O–C=O bonding [54], where the $sp^2$ C=C and $sp^3$ C–C could improve the electrical conductivity and the C–O/C–N, C=O, O–C=O could facilitate the surface hydrophilicity benefiting the aqueous OER process (Fig. 6e and Table S4) [55]. In view of O 1s binding energies, lattice oxygen ($CoO_x$), –OH, and O–C were found in all the samples (Fig. 6f and Table S4) [56]. Notably, $H_2O$/C=O was only detected in TJU-104–900, which was ascribed to its hydrophilic structure to adsorb water ($H_2O$) on the produced C=O functional groups at 900 °C [57]. In brief, by assembling our ultrahigh N-containing ligand, the MOFs could develop a hierarchical structure derivative, *i.e.*, N-doped graphitic carbons encapsulating nano-cobalt particles, with abundant active components (*e.g.*, C–N and C–O groups, specific Co–$N_x$ coordination) driving outstanding OER activity [58]. Meanwhile, in the XPS spectrum of Co after the OER measurement (Fig. S22 in Supporting information), the peaks of Co $2p_{3/2}$ and Co $2p_{1/2}$ apparently shifted to higher binding energies indicating the cobalt active sites might transform to active CoOOH species, which could further facilitate the OER activity [59]. The XRD of the TJU-104–900 after OER implementations was explored to find a new phase ($CoO_3$) generation (Fig. S22).

Through the above investigations, we can rationalize the advantages of our OER catalysts as follows: (1) Higher nitrogen content of the linkers can be conducive to the inherent conductivity of MOFs; (2) N-doped graphitic carbon porous structure could be easily obtained *via* a one-step pyrolysis process from well-defined porous MOFs with high nitrogen content; (3) The obtained hierarchical structure of MOFs derivatives possess functional groups such as graphitic C, N, C=O may increase hydrophilicity of the material surface, and thus facilitate the adsorption of OER intermediates; (4) The coexistence of various valence states of cobalt and Co–$N_x$ could be active catalytic sites to facilitate the OER activity. To sum up, the facile formation of elaborate hierarchical composites from micro-size MOFs synthesized by cheap raw materials and high N-containing organic linkers could be achieved *via* a facile one-step pyrolysis. These MOF derivatives feature novel structures and vari-

ous active components endowing them with superior OER performance to traditional noble-metal materials.

In conclusion, we demonstrated a novel approach to assemble metal and N-doped graphitic carbon composites with hierarchical structure from new MOFs *via* one-step pyrolysis for OER electrocatalysts. Benefiting from the high N-containing linker, the intrinsic conductivity of micro-sized Co-based pristine MOFs could drive high OER activities verified by electrochemical analysis. MOFs derivative TJU-104–900 featuring nano-cobalt particles encapsulated by N-doped graphitic carbon can be readily obtained at 900 °C. The TJU-104–900 inherits the intrinsic conductivity and porous structure of pristine MOFs exhibiting a low overpotential of 280 mV@10 mA/cm$^2$ and outstanding stability for OER activity on carbon cloth. Systematic investigation elucidated that the synergistic effect of various exposed active sites (*e.g.*, Co, $Co_3O_4$, and Co–$N_x$ embedded in graphitic carbons) and hydrophilic porous structure of TJU-104–900 plays a vital role on the electron transportation and conductivity for improved OER performances. This work not only corroborated that the design and synthesis of pristine MOFs with high N-containing linkers is a promising strategy to fabricate excellent electrocatalysts, but also will stimulate researches on one-step pyrolysis of MOFs to prepare novel hierarchical composites for optimal electrocatalysts.

## Declaration of competing interest

The authors declare that they have no known competing financial interests or personal relationships that could have appeared to influence the work reported in this paper.

## Acknowledgments

This work was financially supported by the National Natural Science Foundation of China (Nos. 21875165, 22272118), the Fundamental Research Funds for the Central Universities (No. 22120210529), the Science and Technology Commission of Shanghai Municipality, China (Nos. 22ZR1464100, 19DZ2271500) and the Recruitment Program of Global Experts of China, and Research Grants from the City University of Hong Kong (Nos. CityU 11308420, 6000716, 9667217).

## Supplementary materials

Supplementary material associated with this article can be found, in the online version, at doi:10.1016/j.cclet.2022.108056.

## References

[1] N.T. Suen, S.F. Hung, Q. Quan, et al., Chem. Soc. Rev. 46 (2017) 337–365.
[2] M.G. Walter, E.L. Warren, J.R. McKone, et al., Chem. Rev. 110 (2010) 6446–6473.
[3] G. Zhang, Y. Li, X. Xiao, et al., Nano Lett. 21 (2021) 3016–3025.
[4] C. Niu, Y. Zhang, J. Dong, et al., Chin. Chem. Lett. 32 (2021) 2484–2488.
[5] R. Bashyam, P. Zelenay, Nature 443 (2006) 63–66.
[6] Y. Ren, H. Wang, T. Zhang, et al., Chin. Chem. Lett. 32 (2021) 2243–2248.
[7] Y. Li, H. Dai, Chem. Soc. Rev. 43 (2014) 5257–5275.
[8] M.S. Burke, L.J. Enman, A.S. Batchellor, et al., Chem. Mater. 27 (2015) 7549–7558.
[9] H. Wang, S. Zhu, J. Deng, et al., Chin. Chem. Lett. 32 (2021) 291–298.
[10] C. Wang, L. Jin, H. Shang, et al., Chin. Chem. Lett. 32 (2021) 2108–2116.
[11] Q. Xu, J. Zhang, D. Wang, et al., Chin. Chem. Lett. 2 (2021) 3771–3781.
[12] L. Han, J. Xu, Y. Huang, et al., Chin. Chem. Lett. 32 (2021) 2263–2268.
[13] X.P. Li, C. Huang, W.K. Han, et al., Chin. Chem. Lett. 32 (2021) 2597–2616.
[14] X. Li, X.P. Zhang, M. Guo, et al., J. Am. Chem. Soc. 143 (2021) 14613–14621.
[15] J. Zhu, M. Xiao, Y. Zhang, et al., ACS Catal. 6 (2016) 6335–6342.
[16] W. Li, X. Guo, P. Geng, et al., Adv. Mater. 33 (2021) 2105163.
[17] S. Cao, T. Chen, S. Zheng, et al., Small Methods 5 (2021) 2101070.
[18] Q. Zhang, Y. Wang, Y. Wang, et al., Chin. Chem. Lett. 32 (2021) 3807–3810.
[19] W. Cheng, X. Zhao, H. Su, et al., Nat. Energy 4 (2019) 115–122.
[20] Q. Shi, S. Fu, C. Zhu, et al., Mater. Horiz. 6 (2019) 684–702.
[21] Y. Qian, I.A. Khan, D. Zhao, Small 13 (2017) 1701143.
[22] X. Li, B. Lv, X.P. Zhang, et al., Angew. Chem. Int. Ed. 61 (2022) e202114310.
[23] J. Du, F. Li, L. Sun, Chem. Soc. Rev. 50 (2021) 2663–2695.
[24] X. Liu, L. Dai, Nat. Rev. Mater. 1 (2016) 16064.
[25] S. Gadipelli, T. Zhao, S.A. Shevlin, et al., Energy Environ. Sci. 9 (2016) 1661–1667.
[26] X. Li, Y. Fang, X. Lin, et al., J. Mater. Chem. A 3 (2015) 17392–17402.
[27] Y. Yang, Z. Lun, G. Xia, et al., Energy Environ. Sci. 8 (2015) 3563–3571.
[28] X. Ma, X. Zhao, J. Huang, et al., ACS Appl. Mater. Interfaces 9 (2017) 21747–21755.
[29] Y. Gu, L. Miao, Y. Yin, et al., Chin. Chem. Lett. 32 (2021) 1491–1496.
[30] T. Wang, Y. He, Y. Liu, et al., Nano Energy 79 (2021) 105487.
[31] H. Zhou, M. Zheng, H. Tang, et al., Small 16 (2020) 1904252.
[32] Z. Lei, Y. Tan, Z. Zhang, et al., Nano Res. 14 (2020) 868–878.
[33] W. Zhang, X. Yao, S. Zhou, et al., Small 14 (2018) 1800423.
[34] I.S. Amiinu, X. Liu, Z. Pu, et al., Adv. Funct. Mater. 28 (2018) 1704638.
[35] X.F. Lu, P.Q. Liao, J.W. Wang, et al., J. Am. Chem. Soc. 138 (2016) 8336–8339.
[36] J. Zhao, J.J. Zhang, Z.Y. Li, et al., Small 16 (2020) 2003916.
[37] E. Raymundo-Piñero, M. Cadek, F. Béguin, Adv. Funct. Mater. 19 (2009) 1032–1039.
[38] P. Yin, T. Yao, Y. Wu, et al., Angew. Chem. Int. Ed. 55 (2016) 10800–10805.
[39] G. Yu, J. Sun, F. Muhammad, et al., RSC Adv. 4 (2014) 38804–38811.
[40] X. Hou, H. Zhou, M. Zhao, et al., ACS Sustain. Chem. Eng. 8 (2020) 5724–5733.
[41] B.Y. Xia, Y. Yan, N. Li, et al., Nat. Energy 1 (2016) 15006.
[42] Z.H. Sheng, L. Shao, J.J. Chen, et al., ACS Nano 5 (2011) 4350–4358.
[43] X. Li, H. Wang, J.T. Robinson, et al., J. Am. Chem. Soc. 131 (2009) 15939–15944.
[44] H. Lu, H. Zhang, X. Zhang, et al., Appl. Surf. Sci. 448 (2018) 369–379.
[45] Q. Ren, H. Wang, X.F. Lu, et al., Adv. Sci. 5 (2018) 1700515.
[46] J. Zhang, L. Dai, ACS Catal. 5 (2015) 7244–7253.
[47] R. Subbaraman, D. Tripkovic, K.C. Chang, et al., Nat. Mater. 11 (2012) 550–557.
[48] L. Zhao, B. Dong, S. Li, et al., ACS Nano 11 (2017) 5800–5807.
[49] Y. Shi, Y. Yu, Y. Liang, et al., Angew. Chem. Int. Ed. 58 (2019) 3769–3773.
[50] R. Wu, D.P. Wang, K. Zhou, et al., J. Mater. Chem. A 4 (2016) 13742–13745.
[51] W. Zheng, M. Liu, L.Y.S. Lee, ACS Catal. 10 (2020) 81–92.
[52] J. Casanovas, J.M. Ricart, J. Rubio, et al., J. Am. Chem. Soc. 118 (1996) 8071–8076.
[53] W. Wu, Q. Zhang, X. Wang, et al., ACS Catal. 7 (2017) 7267–7273.
[54] S. Li, W. Chen, H. Pan, et al., ACS Sustain. Chem. Eng. 7 (2019) 8530–8541.
[55] F. Sun, G. Wang, Y. Ding, et al., Adv. Energy Mater. 8 (2018) 1800584.
[56] X.C. Li, F.S. She, D. Shen, et al., RSC Adv. 8 (2018) 28625–28631.
[57] K. Fan, H. Zou, Y. Lu, et al., ACS Nano 12 (2018) 12369–12379.
[58] S.N. Faisal, E. Haque, N. Noorbehesht, et al., RSC Adv. 7 (2017) 17950–17958.
[59] J. Huang, J. Chen, T. Yao, et al., Angew. Chem. Int. Ed. 54 (2015) 8722–8727.